Elsevier Editorial System(tm) for Earth and Planetary Science Letters
Manuscript Draft

Manuscript Number: EPSL-D-10-00140R1

Title: Direct evidence for upper mantle structure in the NW Pacific Plate: microstructural analysis of a petit-spot peridotite xenolith

Article Type: Regular Article

Keywords: petit-spot; peridotite xenolith; crystallographic preferred orientation (CPO); seismic anisotropy; Northwestern Pacific Plate; lithosphere-asthenosphere boundary

Corresponding Author: Dr Yumiko Harigane,

Corresponding Author's Institution: Kanazawa University

First Author: Yumiko Harigane

Order of Authors: Yumiko Harigane; Tomoyuki Mizukami; Tomoaki Morishita; Katsuyoshi Michibayashi; Natsue Abe; Naoto Hirano

Abstract: Petit-spots, the late Miocene alkali basaltic volcanoes on the Early Cretaceous NW Pacific Plate, originate at the base of the lithosphere. The petit-spot volcanic rocks enclose fragments of tholeiitic basalt, dolerite, gabbro, and mantle peridotite, providing a unique window into the entire section of subducting oceanic lithosphere. We provide here the first direct observations on the deep structure of the Pacific lithosphere using microstructural analyses of a petit-spot peridotite xenolith. The xenolith is a lherzolite that consists mainly of coarse- and medium-grained olivine, orthopyroxene, and clinopyroxene, as well as fine-grained aggregates of spinel and orthopyroxene that probably represent replaced pyrope-rich garnet. A strong deformational fabric is marked by a parallel alignment of millimeter-sized elongate minerals and their crystallographic preferred orientation. The olivine displays an [010] fiber pattern with a girdle of [100] axes and a maximum of [010] perpendicular to the foliation, a pattern which is consistent with a transpressional deformation in high temperature conditions at the base of oceanic lithosphere. Our microstructural observations and seismic data indicate that the lower part of the NW Pacific lithosphere possess an early stage structure of mantle flow at the asthenosphere. This interpretation is compatible with a conventional model in which oceanic lithosphere is thickened during cooling and plate convection. A discrepancy between the weak anisotropy in the petit-spot peridotite and the strong azimuthal anisotropy from the seismic data in the NW Pacific plate implies the existence of a highly anisotropic component in the deep oceanic lithosphere.

Direct evidence for upper mantle structure in the NW Pacific Plate: microstructural analysis of a petit-spot peridotite xenolith

Yumiko Harigane[a*], Tomoyuki Mizukami[b], Tomoaki Morishita[a], Katsuyoshi Michibayashi[c], Natsue Abe[d], Naoto Hirano[e]

[a]*Frontier Science Organization, Kanazawa University, Kanazawa 920-1192, Japan*
[b]*Department of Earth Science, Graduate School of Environmental Studies, Kanazawa University, Kanazawa 920-1192, Japan*
[c]*Institute of Geosciences, Shizuoka University, Shizuoka 422-8529, Japan*
[d]*Institute for Research on Earth Evolution, Japan Agency for Marine-Earth Science and Technology, Kanagawa 236-0016, Japan*
[e]*Center for Northeast Asian Studies, Tohoku University, Sendai, 980-8576, Japan*

*Corresponding author. Tel: +81-76-264-6539; Fax: +81-76-264-6545;
E-mail address: harigane@staff.kanazawa-u.ac.jp (Y. Harigane)

Abstract

Petit-spots, the late Miocene alkali basaltic volcanoes on the Early Cretaceous NW Pacific Plate, originate at the base of the lithosphere. The petit-spot volcanic rocks enclose fragments of tholeiitic basalt, dolerite, gabbro, and mantle peridotite, providing a unique window into the entire section of subducting oceanic lithosphere. We provide here the first direct observations on the deep structure of the Pacific lithosphere using microstructural analyses of a petit-spot peridotite xenolith. The xenolith is a lherzolite that consists mainly of coarse- and medium-grained olivine, orthopyroxene, and clinopyroxene, as well as fine-grained aggregates of spinel and orthopyroxene that probably represent replaced pyrope-rich garnet. A strong deformational fabric is marked by a parallel alignment of millimeter-sized elongate minerals and their crystallographic preferred orientation. The olivine displays an [010] fiber pattern with a girdle of [100] axes and a maximum of [010] perpendicular to the foliation, a pattern which is consistent with a transpressional deformation in high temperature conditions at the base of oceanic lithosphere. Our microstructural observations and seismic data indicate that the lower part of the NW Pacific lithosphere possess an early stage structure of mantle flow at the asthenosphere. This interpretation is compatible with a conventional model in which oceanic lithosphere is thickened during cooling and plate convection. A discrepancy between the weak anisotropy in the petit-spot peridotite and the strong azimuthal anisotropy from the seismic data in the NW Pacific plate implies the existence of a highly anisotropic component in the deep oceanic lithosphere.

Key wrds: petit-spot, peridotite xenolith, crystallographic preferred orientation (CPO), seismic anisotropy, Northwestern Pacific Plate, lithosphere-asthenosphere boundary

1. Introduction

Oceanic plates cover about 70% of the Earth's surface, and exert a major control on the thermal evolution, material circulation, and dynamics of our planet (Turcotte and Schubert, 1982). Reaching an understanding of the visco-elastic and petrological structures of oceanic plates is one of the most fundamental aims of earth science (McKenzie, 1967; Parsons and Sclater, 1977; Stein and Stein, 1992; Faccenda et al., 2008; Kawakatsu et al., 2009). Tectonic structures in the lithosphere develop progressively from mid-oceanic ridges to convergent margins, eventually influencing the processes of subduction.

A conventional semi-infinite half-space model of heat conduction for the growth of an oceanic plate provides a beautiful explanation for the observed depth profiles of ocean floors and heat flow measurements (e.g., Davis and Lister, 1974; Davies, 1980; Turcotte and Schubert, 1982; Stein and Stein, 1992). Seismic observations have verified the predicted depths of the lithosphere–asthenosphere boundary (LAB), which increase with increasing age of the oceanic plate (Turcotte and Schubert, 1982; Kawakatsu et al., 2009). The results of a recent seismic analysis using a receiver function suggest the existence of a layered melt-rock structure at the top of the asthenosphere (Kawakatsu et al., 2009). These studies indicate that the upper part of an oceanic plate thickens downwards at the LAB as it moves away from a ridge, and that anisotropic structures develop in response to interactions between lithosphere and asthenosphere.

Deformational structures in oceanic lithosphere are important because they enable interpretations of the observed seismic anisotropy in terms of flow directions or plate motions (Nicolas and Christensen, 1987; Savage, 1999; Park and Levin, 2002; Long and Silver, 2009). Based on experiments and geological observations of plastically deformed peridotites, it is generally accepted that the fastest direction of seismic wave propagation represents the direction of mantle flow (Nicolas and Christensen, 1987; Nicolas, 1989; Mainprice et al., 2000). However, geological observations on upper mantle structures in oceanic plates have been restricted to the shallowest part of the mantle, in the spinel-lherzolite facies, corresponding to depths in the upper half of the plates, and it is not known whether the shallow structures are comparable to those in the lower half. Although hotspot xenoliths are potentially derived from deep levels of the sub-oceanic mantle, they are part of a hybrid mantle significantly modified by intra-oceanic plume-related processes, such as those underlying Hawaii (Sen et al., 2005), French Polynesia (Tommasi et al., 2004), the Canaries (Vonlanthen et al., 2006), and Kerguelen (Bascou et al., 2008).

Recently, a new window into oceanic lithosphere has been discovered on the seafloor of the NW Pacific. It is called a petit-spot, a new type of intra-plate volcanism caused by flexing of an oceanic plate upon entering the Japanese subduction zone (Hirano et al., 2006). Petrological studies reveal that the alkali basaltic volcanoes have their roots at the base of the NW Pacific lithosphere (Hirano et al., 2006, 2008), and that essentially unaltered pieces of oceanic lithosphere were caught up in the ascending magma as mafic and ultramafic xenoliths (Hirano et al., 2004; Abe et al., 2006; Yamamoto et al., 2009).

During focused and exhaustive investigations of the NW Pacific petit-spot knolls, Abe et al. (2006) reported the discovery of a centimeter-sized peridotite fragment that had originated in the garnet-stability field. Here, we report the results of a microstructural analysis of this petit-spot xenolith; based on the results of the analysis, we go on to infer the structure and evolution of the Pacific Plate. Even though the sample is small, containing a limited number of grains, it possibly represents great importance as a natural sample of the widespread deeper parts of the Pacific lithosphere.

2. Sample locality and petrological background

The petit-spot volcanoes are located on the seaward slope of the northern Japan Trench (Fig. 1). The NW Pacific Plate is Early Cretaceous in age (150–120 Ma), making it the oldest oceanic plate in the world. However, geochronological data reveal that the petit-spot alkali basaltic volcanism occurred during the late Miocene to present (Hirano et al., 2001, 2006, 2008). Reconstructions of recent plate motion show that the locus of volcanism was on the seaward slope of the outer rise, indicating that the young basalts were erupted along lithospheric fractures in response to plate flexure during subduction (Hirano et al., 2006). The silica-undersaturated nature and LREE-enriched geochemical signature of the alkali basalts are compatible with a small degree of partial melting of mantle beneath the LAB (Hirano et al., 2001, 2006).

Some mafic xenocrysts and xenoliths of tholeiitic basalt, dolerite, gabbro and mantle peridotite were obtained from the petit-spot volcanoes, which are typically monogenetic alkali basalt volcanoes (Abe et al., 2006). The mantle peridotite xenoliths consist of lherzolite and olivine orthopyroxenite. The major element data for the constituent minerals in the petit-spot peridotite xenoliths are presented by Abe et al. (2006) and Yamamoto et al. (2009). The Fo (forsterite) values [Mg/(Mg + Fe) × 100] of olivine are 89.8–92.7, slightly higher than those of typical mantle (e.g., Takahashi, 1986; Arai, 1994). The Cr# [Cr/(Cr + Al)] of spinel in the petit-spot peridotite xenoliths varies from 0.08 to 0.38 (Abe et al., 2006; Yamamoto et al., 2009). These values suggest that the source mantle had already been molten to some degree. Using a two-pyroxene geothermometer (Wells, 1977) and CO_2 Raman densimeter (Yamamoto and Kagi, 2006), equilibrium conditions of spinel and garnet peridotites were determined to be 800–1100 °C at a minimum pressure of 13–16 kbar, corresponding to a depth of >40–50 km below the seafloor (Abe et al., 2006; Yamamoto et al., 2009). Generation of mid-ocean ridge basalt (MORB) could be considered as a possible depletion event in sub-oceanic mantle. Noble gas isotopic data for three spinel lherzolite xenoliths and two sets of olivine xenocrysts in three submarine volcanoes indicate that the xenoliths resemble MORB (Yamamoto et al., 2009).

The sample analyzed here is the very fresh peridotite xenolith enclosed in a highly vesicular alkali basalt (up to 2 cm in diameter; 6K#880R2O; Fig. 2), that was obtained during the cruise YK05-06, R/V *Yokosuka* and the submersible *Shinkai 6500* from a dive site 6K#880 at the eastern fault escarpment of a petit-spot volcano in the Japan Trench (Fig. 1; Site A of Hirano et al., 2006). The petit-spot peridotite xenolith is lherzolite consisting of olivine, orthopyroxene and clinopyroxene (Fig. 3a, b). The mean Fo value of olivine is 91.4, indicating a relatively undepleted nature. The petit-spot peridotite xenolith contains fine-grained spinel-orthopyroxene aggregates with minor glass (Fig. 4b, c). The Al_2O_3 contents of orthopyroxene and the Cr# [Cr/(Cr + Al)] of spinel range widely from 4 to more than 15 wt% and from 0.1 to 0.24, respectively. The rounded shapes of the aggregates and their bulk chemical compositions (determined by a defocused beam) are consistent with an origin of pyrope-rich garnet. The bulk trace-element patterns of the aggregates are similar to those of pyrope-rich garnet and the associated clinopyroxene shows a signature typically seen in those equilibrated under conditions of the garnet-lherzolite stability field (Abe et al., 2006).

The equilibrium conditions of this sample applied to a two-pyroxene geothermometer (Wells, 1977) and a univariant curve for the garnet-spinel facies transition (O'Neill, 1981; Klemme and O'Neill, 2000), indicating that was determined to be 1100±50 °C at a pressure of 16-20 kbar. This conditions correspond to a depth of ~60 km below the seafloor (Abe et al., 2006; Yamamoto et al., 2009).

3. Microstructure and mineral preferred orientation

Microstructure of the petit-spot peridotite xenolith (6K#880R2O) was examined in two vertical sections (A and B sections in Fig. 2). Strong shape preferred orientations (SPO) in these sections indicate the foliated structure of the peridotite (Fig. 2 and 3). The X direction is approximately parallel to the mineral SPO in the A section and the XZ plane is oblique to the A section with a dihedral of about 30º (Fig. 2).

The microstructure is characterized by a coarse granular (partly tabular) texture that consists dominantly of coarse olivine and medium-grained pyroxenes (Fig. 3a, b). Elongate olivine grains define a lineation. Almost orthopyroxene and clinopyroxene grains are elongate and sub-parallel to the elongate olivine grains (Fig. 3a, b). Olivine grains show features of intra-crystalline deformation, including subgrain boundaries and extremely high aspect ratios (Figs. 3 and 4a). Wavy extinction and deformational twinning is not observed in the pyroxenes. The SPO of the crystals seems to be orthogonal in symmetry, and subgrains are not conspicuously oblique (Fig. 3a, b). A reaction zone between the host rock and peridotite could be observed at the contact between the host rock and peridotite (Fig. 3a, b).

The spinel-orthopyroxene aggregates after pyrope-rich garnet shows a rounded shape. The inner parts of the aggregates are very fine-grained, with many cracks, whereas the outer parts are coarser-grained with a granular texture, indicating that the garnet decomposed as a result of at least two processes with different reaction rates (Fig. 4b, c). The concentric structure within the garnet pseudomorphs indicates that the breakdown postdates the major deformation of the peridotite.

We analyzed the orientation of olivine and two-pyroxene grains in highly polished thin sections using a scanning electron microscope (SEM; JEOL JSM6300) equipped with an electron-backscatter diffraction (EBSD) system at the Center for Instrumental Analysis, Shizuoka University. Operating conditions were as follows: accelerating voltage 20 kV, probe current 10 nA, working distance 24 mm, and tilt angle 70°. All index data represent points with a mean angular deviation (MAD) of <1°. Errors in computed indexation of each diffraction pattern were verified by the operator. The olivine orientation map of the peridotite was collected with a step size of 50 μm.

The orientations of crystallographic axes of olivine, orthopyroxene, and clinopyroxene are presented in equal-area, lower-hemisphere projections (Fig. 5a). We measured the crystal orientations of 191 olivine grains, 100 orthopyroxene grains and 17 clinopyroxene grains, merging the data from two parallel thin sections of the A section in the sample 6K880R2O (Fig. 2). The crystallographic preferred orientation (CPO) of olivine shows a girdle of [100] and [001] axes within the foliation and a point maximum of [010] perpendicular to the foliation (Fig. 5a). The CPO of orthopyroxene forms a girdle of [001] almost concordant with the girdles of olivine [100] and [001] (Fig. 5a) whereas other axes do not show distinct patterns. The similarity in patterns of olivine [001] and orthopyroxene [001] orientations suggests coincident formation of the CPOs. The CPO of clinopyroxene could not be confirmed because of the small number of grains (Fig. 5a).

An orientation map for the petit-spot peridotite xenolith is shown in Figure 3c. The color of olivine is defined by its orientation; for example, a grain with its [100] axis oriented sub-parallel to the lineation is blue, but a grain with [001] parallel to the lineation is red (Fig.3c). Orthopyroxene, clinopyroxene and undetermined olivine are shown as white areas in the figure. Olivine grains with [100] parallel to the lineation (Fig. 3c; blue-colored grains) are dominant and are more elongate than grains with [001] parallel to the lineation (Fig. 3c; red-colored grains). The purple-colored grains are observed at the orientation map (Fig. 3c) and are oriented in directions between [100] and [001] (Fig. 3c). The olivine grains of upper area in thin section are relatively coarser grain than that of lower area. In the orientation map, each grain on upper area has similar orientation with [100] and a direction between [100] and [001] parallel to lineation, whereas the grain on lower area shows a different orientation in each grain.

Subgrain boundaries are characteristically observed in olivine grains with [100] parallel to the lineation. We used a rotation axis method to determine the slip system in the olivine grains (e.g., Mehl et al., 2003; Satsukawa and Michibayashi, 2009). We measured olivine crystal orientations across several subgrain boundaries, or tilt walls. Since tilt walls are formed of edge dislocations, the orientation of the tilt wall and the lattice rotation across that tilt wall can be presented the dominant slip system (e.g., Mehl et al., 2003; Satsukawa and Michibayashi, 2009). The results indicate slip on the (010)[100] system. This is the most common slip system in naturally deformed olivine (e.g., Nicolas and Poirier, 1976), and experimental studies reveal that this system is the most active at high temperatures (>1100 °C; e.g., Nicolas et al., 1973; Avé Lallemant, 1975; Nicolas and Christensen, 1987; Zhang and Karato, 1995; Zhang et al., 2000; Jung et al., 2006).

4. Seismic properties of the petit-spot peridotite

Seismic properties of the petit-spot peridotite xenolith were calculated from single crystal elastic constants, density and the CPO of olivine, enstatite and diopside. We inputted the parameters of average modal composition: olivine (78.9 %), orthopyroxene (12.8 %), and clinopyroxene (8.3 %), the EBSD-measured CPO of major minerals (olivine, orthopyroxene and clinopyroxene), and the elastic constants of olivine, orthopyroxene and clinopyroxene at 20 kbar and 1100ºC and we used a Voigt-Reuss-Hill average scheme (Mainprice et al., 2000). The elastic constants used in our calculations are those of Abramson et al. (1997) for olivine, Chai et al. (1997) for enstatite, and Collins and Brown (1998) for diopside. The P-wave anisotropy was calculated as a percentage using the formula $200(Vp^{max}-Vp^{min})/(Vp^{max}+Vp^{min})$. The S-wave anisotropy (AVs) was calculated for a specific propagation direction using the formula $200(Vs_1-Vs_2)/(Vs_1+Vs_2)$, where Vs_1 and Vs_2 are the fast and slow wave velocities, respectively (e.g., Pera et al., 2003, Tasaka et al., 2008).

The results of our calculations are shown in Figure 5b. The P-wave velocity (Vp) is fastest (8.3 km/s) subparallel to the lineation, which is closely related to the CPO maximum of olivine [100] axes (Fig. 5b). The P-wave velocity (Vp) is slow (7.53 km/s) for waves propagating in a plane normal to the [100] maximum (Fig. 5b). The P-wave anisotropy is 9.7 % between fast (8.3 km/s) and slow (7.53 km/s) P-wave velocities. Fast split shear wave velocity (Vs_1) is max 4.77 km/s and slow split shear wave velocity (Vs_2) is max 4.52 km/s. Polarization anisotropy of S-wave (AVs) is max

8.3 % and shows two maxima on a girdle parallel to the girdle of [100] axes (Fig. 5b). The orientation of the polarization plane of the fastest S-wave systematically (Vs1 polarization plane) marks the orientation of the great circle that contains the maximum concentration of [100] (Fig. 5b).

5. Discussion

5.1. Microstructural development of the petit-spot peridotite xenolith

The microstructure of the petit-spot peridotite xenolith is characterized by i) a coarse granular texture with a strong SPO and ii) an olivine CPO with [010] concentrated normal to the foliation and [100] in a girdle normal to the [010] maximum (Figs. 3 and 5a). The olivine CPO is compatible with the [010] fiber pattern (or AG-type) described by Ben Ismail and Mainprice (1998) and Mainprice (2007), among others, and the pattern indicates the nature of the main deformational phase of the petit-spot peridotite xenolith. The development of sub-grain boundaries is rather local and there is no sign for a transition to a porphyroclasic microstructure, indicating the peridotite has not been affected by high strain and/or lower temperature overprinting that is often observed in mantle sections of ophiolites (e.g., Nicolas, 1986; Suhr, 1993).

The P–T estimate of 16–20 kbar minimum pressure and 1100±50 °C for the petit-spot peridotite xenolith, as obtained using the garnet–spinel transition in lherzolite (Abe et al., 2006; Yamamoto et al., 2009), constrains the equilibrium conditions just before entrainment of the xenolith by the petit-spot magma. These conditions are consistent with slip on (010)[100], as determined by our analysis of subgrain rotation axes. The fact that garnet pseudomorphs in the petit-spot peridotite xenolith have retained their isochemical characteristics (Fig. 4b) indicates that the main deformation associated with the [010] fiber pattern in olivine took place while the garnet was stable. This requires higher pressure or lower temperature conditions for the formation of the [010] fiber pattern than the pressures and temperatures estimated above. Considering the geochemical signature for MORB extraction (Yamamoto et al., 2009) and passive transport by plate motion, it is reasonable to assume that the petit-spot peridotite xenolith retained a largely consistent vertical position in the Pacific Plate during its tectonic evolution.

Although the [010] fiber pattern in natural peridotites is relatively uncommon worldwide ([010] fiber pattern in percentages of the database is 10.1%; Ben Ismaïl and Mainprice, 1998; Mainprice, 2007), it is reported from many localities in various tectonic settings. For example, it is found in alpine peridotite, as in the Ronda (Vauchez and Garrido, 2001) and Lherz peridotite massifs (Le Roux et al., 2007, 2008), in cratonic kimberlite xenoliths (Ben Ismail et al., 2001; Vauchez et al., 2005), and in sub-continental mantle xenoliths from SE Siberia (Tommasi et al., 2008). The [010] fiber pattern is also observed in the subduction-related orogen of the Canadian Cordillera (Tommasi et al., 2006) and in xenolith samples from the intra-oceanic settings of the Canaries (Vonlanthen et al., 2006) and Kerguelen (Bascou et al., 2008). The local occurrence of this high-temperature deformation pattern in the Hilti massif of the Oman ophiolite (Michibayashi and Mainprice, 2004) represents a rare example from oceanic lithosphere. In the following, previously proposed five mechanisms will be examined as the cause of the [010] fiber pattern in the petit-spot peridotite xenolith.

First, the [010] fiber pattern may develop during axial compression (Nicolas et al., 1973). In this case, the concentration of [010] parallel to the compression axis increases with strain. However, this mechanism is not consistent with the concentration of the orthopyroxene [001]-axis in the petit-spot peridotite xenolith (Fig. 5a); furthermore, it is unlikely to occur within oceanic lithosphere, where an intense simple shear to accommodate mantle flow is expected (e.g., Nicolas, 1989; Michibayashi and Mainprice, 2004).

Second, a numerical study indicated that the [010] fiber pattern could result from a transpressional deformation dominated by the single slip system (010)[100] (Tommasi et al., 1999). Dispersion of olivine [100] and orthopyroxene [001] axes within the foliation plane is expected under this mechanism (e.g., Vauchez and Garrido, 2001; Tommasi et al., 2006; Bascou et al., 2008). In the petit-spot peridotite xenolith, the orthopyroxene grains are characterized by a girdle of [001] and a weak maximum of [100] (Fig. 5a), suggesting that the observed olivine [010] fiber pattern could have resulted from transpressional shear deformation.

Third, the simultaneous activation of [100] and [001] slip directions under high-stress or high-pressure conditions is a possible mechanism for forming a [010] fiber pattern (Tommasi et al., 2000; Mainprice et al., 2005). This mechanism has been invoked to explain the [010] fiber patterns in deep-rooted cratonic xenoliths (Vauchez et al., 2005; Tommasi et al., 2008). However, for the studied sample, all the observed tilt boundaries in olivine grains indicate a [100](010) slip system. The petit-spot peridotite xenolith is considered to have been deformed under conditions close to the garnet–spinel transition, which is too shallow to have activated multiple slip directions (Mainprice et al., 2005; Jung et al., 2008).

Sub-grain rotation due to dynamic recrystallization is a possible fourth explanation (Tommasi et al., 2000). A diffusion of the CPO due to subgrain rotation counterbalances the CPO intensification due to dislocation glide, resulting in a steady-state fabric similar to the [010] fiber pattern. However, in the petit-spot peridotite xenolith, rotation of crystallographic axes appears to be minor in a single grain and oblique fabric is not seen. There is no microstructural evidence that sub-grains in olivine turn to form neoblasts through dynamic recrystallization.

The fifth possible mechanism was discovered during experimental deformation, when strain partitioning in a partially molten peridotite produced a weak [010] fiber pattern (Holtzman et al., 2003). A similar mechanism has been proposed by Le Roux et al. (2007, 2008) and Tommasi et al. (2008). Tommasi et al. (2008) emphasized the roles of annealing and static recrystallization associated with melt percolation; the authors applied this mechanism to Siberian mantle xenoliths with coarse-grained, annealed microstructures and [010] fiber patterns. These microstructural features (Tommasi et al., 2008) are similar to those of the petit-spot peridotite xenolith. An orthogonal symmetry characterizes the structure of the petit-spot peridotite xenoliths, and a similar structure has been reported in deformed partially molten peridotite, where the shear component of strain is accommodated by interstitial melt (e.g., Zimmerman et al., 1999; Holtzman et al., 2003). Yamamoto et al. (2009) suggested that the source mantle of the petit-spot magma had already been molten to some degree, whereas the peridotite xenolith of this study shows no direct petrological evidence for the existence of silicate melts or fluids during the formation of the [010] fiber pattern.

As discussed above, the microstructures can be interpreted by two mechanisms: transpressional strain and presence of partial melt. A large-scale transpressional deformation is expected in a horizontally extending flow in which a thinning is dominant. One possible site is in a plume head beneath oceanic lithosphere (e.g., Ernst and Buschan, 2003). However, the geochemical characteristics of the peridotite indicate a MORB source mantle (Yamamoto et al., 2009). Local transpressional strain can be achieved in high temperature deformation if a bulk shear is compensated by soft layers or slip boundaries. This is, in turn, a mechanical explanation for [010] fiber patterns in partially molten rocks (Holtzman et al., 2003). This leads us to considering high temperature deformation in a presence of partial melt over the others for the formation of the [010] fiber pattern in olivine of the petit-spot xenolith. A recent asthenosphere model based on receiver function analyses (Kawakatsu et al., 2009) and the less depleted geochemical nature (Abe et al, in prep.) are compatible with solid layers intercalated with melt-rich layers.

5.2. Upper mantle structure beneath the NW Pacific Sea

The layered elastic structure beneath the NW Pacific Sea has been examined through long-range explosion seismic experiments using ocean bottom seismometer and a borehole broadband observatory at the NW Pacific basin (Shimamura et al., 1983; Shinohara et al., 2008). Of course, it is impossible to restore the petit-spot peridotite xenolith to its original orientation before it was transported to the surface; however, the mantle piece provide a test for interpretations on the formation of the velocity structure and the intrinsic anisotropy of the oceanic upper mantle.

Long-range seismic refraction surveys during 1974–1980 revealed the lithospheric mantle of the NW Pacific Plate indicated the two layers of different P-wave velocities at the lithospheric mantle: 8.0–8.2 km/s in the shallower layer and 8.6 km/s in the deeper layer (Shimamura et al., 1983). The interface between the low- and high-velocity layers in the lithospheric mantle of NW Pacific Plate lies at a depth of approximately 40–50 km below the seafloor at the east of the Japan trench (Shimamura et al., 1983; Shimamura and Asada, 1984) although some seismic studies could not detect anisotropy of P-wave velocity (Nagumo et al., 1990; Ouchi and Nagumo, 1990). Recently, the estimated P-wave velocities of uppermost mantle beneath the WP-2 in order to investigate to construct the seismic structure of upper mantle in the NW Pacific Plate (WP-2; a seafloor borehole of the ODP Leg191; Shinohara et al., 2008) range from 8.0 to 8.4 km/s. Shinohara et al. (2008) reported that the 8.5 km/s layer underlies the uppermost mantle layer with a P-wave velocity of 8.3 km/s for fast direction. This interface located at the depth of 30 km below the NW Pacific Plate by Nagumo et al. (1990) and Ouchi and Nagumo (1990).

In Shimamura et al. (1983), the fast direction of the maximum P-wave velocity (8.6 km/s) trends 150–160° from north, perpendicular to the stripes of the paleo-magnetic field on the NW Pacific. The observed direction of the maximum P-wave velocity is parallel to the paleo-spreading direction of the Pacific Plate prior to the change in plate motion that occurred at about 50 Ma (e.g., Shimamura et al. 1983; Molnar and Stock, 1987; Sharp and Clague, 2006). The fast direction of maximum P-wave velocity is also approximately 140º perpendicular to the magnetic lineations (140º) as reported by Shinohara et al. (2008). This result is relatively consistent with those of Shimamura et al. (1983), indicating that the fast direction of maximum P-wave velocity throughout lithospheric mantle is inherited from the past plate motion. The magnitudes of the P-wave and the S-wave anisotropy in the uppermost mantle beneath the WP-2 are 5% and 3.5%, respectively (Shinohara et al., 2008). Travel times of earthquakes recorded by the WP-2 and the previous seismological studies (Nagumo et al., 1990; Ouchi and Nagumo, 1990) suggest that the lower part of the Pacific lithosphere has greater anisotropy than the upper part of the Pacific lithosphere (see Fig. 17 in Shinohara et al. 2008). The deeper part of the lithospheric mantle is also characterized by the strong P-wave velocity anisotropy (13%) in Shimamura et al. (1983).

The maximum P-wave velocity calculated from the CPO of olivine, orthopyroxene and clinopyroxene in the petit-spot peridotite xenolith show 8.3 km/s parallel to lineation (Fig. 4b). This P-wave velocity is slower than the seismic data obtained from seismic experiments beneath the NW Pacific (Shinohara et al., 2008). The fast direction of maximum P-wave velocity (8.30 km/s) coincident with the flow direction is likely to have oriented toward approximately 140º, that is perpendicular to the magnetic lineations for paleo-spreading ridge. Assuming that the foliation is oriented sub-parallel to the plate in order to infer the orientation of mantle flow, the strength of anisotropy calculated from the perit-spot peridotite xenolith is less than ~2 %. Such weak anisotropy of the petit-spot peridotite xenolith exhibits a discrepancy from the strong horizontal anisotropy in the lower part of Pacific lithosphere (up to 13%), implying that an unknown highly anisotropic component lies in the deep oceanic lithosphere in addition to the peridotite with the olivine [010] fiber pattern. Such a hybrid lithosphere might be formed through a solidification of a partially molten layered asthenosphere (Kawakatsu et al., 2009).

The lower limit of the lithosphere is defined by a transition to a low velocity zone representing asthenosphere where the depth of the LAB in the NW Pacific at around 80 km was reported from Shimamura and Asada (1984) and Kawakatsu et al. (2009). Kawakatsu et al. (2009) also revealed that the depth for LAB beneath the Pacific Plates is age-dependent using the data from borehole broadband ocean bottom seismometers. They concluded that the relative thickness of oceanic plate is consistent with the thermally controlled origin for the oceanic LAB (see Fig. 4A in Kawakatsu et al.. 2009). The minimum pressure condition for the garnet-bearing mineral assemblage in the petit-spot peridotite xenolith indicates the origin deeper than about ~60 km (Abe et al., 2006). The microstructural and petrological observations in the petit-spot peridotite xenolith imply that the structures, at least in the lower half of the NW Pacific Plate, were fixed during the early stages of plate thickening. In order to preserve such high temperature fabric during cooling of the lithosphere, a shear strain should be localized to the LAB.

To understand the cause and mechanism for the strong anisotropy in the deep part of oceanic lithosphere, further sampling of mantle pieces from the depths of 30-80 km is necessary. We believe that the first finding of such a peridotite xenolith is an important step for practical understanding of the whole section of the oceanic plate.

6. Concluding remarks

Petit-spot volcanoes on the NW Pacific ocean floor provide us a unique opportunity to touch the lithospheric materials subducting beneath the present Eurasian margin. We made microstructural analyses of a remarkable petit-spot peridotite xenolith, which is petrologically ascertained as a pristine fragment of the oceanic lithosphere deeper than 60 km below the seafloor. The CPO of minerals in the petit-spot peridotite xenolith explains the seismic properties in the deep high-velocity layer of the Pacific lithosphere, including the magnitude of the P-wave velocity and the nature of the layer's anisotropy. Given that the fastest direction in P-wave velocity is parallel to the ancient spreading direction, it can be deduced that the anisotropy was produced by lithosphere–asthenosphere interaction during plate convection. This interpretation is consistent with our finding of the olivine [010] fiber pattern that could be related to the shear deformation in a presence of partial melt. The occurrence of such a fabric, which is a relic of earlier conditions in the garnet stability field, suggests the preservation of an earlier structure as a result of weak coupling at the LAB.

The information gleaned from the peridotite xenolith is likely to fit the general structure of the Pacific Plate and provides a practical understanding for conventional plate model with static growth during cooling. Our first result from petit-spot peridotite xenolith exhibits the importance of taking into account olivine [010] fiber patterns in any interpretation of the global seismic structure of oceanic lithosphere.

Acknowledgements

We thank the captains and crews of the R/V *Yokosuka* and the submersible *Shinkai 6500*, and the science parties during cruises YK05-06 for their support and cooperation. We appreciate the help of T. Fujiwara in drafting the map shown in Figure 1. The figures showing CPO and seismic property data were made using the interactive programs of David Mainprice of Université Montpellier II, France. This study made use of analytical instruments (SEM-EBSD system) housed at the Center for Instrumental Analysis, Shizuoka University, Japan. We thank Aaron Stallard, University of Canterbury, New Zealand, for improving the English of the manuscript. The study was supported by research grants awarded to T. Mizukami (20549003), T. Morishita (21403010), KM (19340148 and 16340151), and NA (17340136 and 20340124) from the Japan Society for the Promotion of Science.

References

Abe, N., Yamamoto, J., Hirano, N., Arai, S., 2006. Petrology and geochemistry of mantle xenoliths from petit-spot volcano, NW Pacific Plate. Geochim. Cosmochim. Acta. 70, A1.

Abramson, E. H., Brown, J. M., Slutsky, L. J., Zang, J. J., 1997. The elastic constants of San Carlos olivine to 17 GPa. J. Geophys. Res. 102, 12253–12263.

Amante, C., Eakins, B.W., 2008. ETOPO1 1 Arc-Minute Global Relief Model. Procedures, Data Sources and Analysis, National Geophysical Data Center, NESDIS, NOAA, U.S. Department of Commerce, Boulder, CO, August 2008.

Arai, S., 1994. Characterization of spinel peridotites by olivine-spinel compositional relationships: review and interpretation. Chem. Geol. 113, 191–204.

Avé-Lallemant, H. G., 1975. Mechanisms of preferred orientations in olivine in tectonite peridotites. Geology 3653-3656.

Bascou, J., Delpech, G., Vauchez, A., Moine, B.N., Cottin, J.Y., Barruol, G., 2008. An integrated study of microstructural, geochemical, and seismic properties of the lithospheric mantle above the Kerguelen plume (Indian Ocean). Geochem. Geophys. Geosyst. 9, Q04036, doi:10.1029/2007GC001879.

Ben Ismail, W., Mainprice, D., 1998. An olivine fabric database: an overview of upper mantle fabrics and seismic anisotropy. Tectonophysics 296, 145-157.

Ben Ismail, W., Barruol, G., Mainprice, D., 2001. The Kaapvaal craton seismic anisotropy: petrophysical analyses of upper mantle kimberlite nodules. Geophys. Res. Lett. 28 (13), 2497–2500.

Carter, N. L., 1976. Steady state flow of rocks. Rev. Geophys. Space Phys., 14, 301-360.

Chai, M., Brown, J. M., Slutsky, L. J., Zang, J., 1997. The elastic constants of an aluminous orthopyroxene to 12.5 GPa. J. Geophys. Res. 102, 14779– 14785.

Collins, M. D., Brown, J. M., 1998. Elasticity of an upper mantle clinopyroxene. Phys. Chem. Miner. 26, 7 – 13.

Crosson, R. S., Lin, J. W., 1971. Voigt and Reuss prediction of anisotropic elasticity of dunite, J. Geophys. Res. 76, 570–578, doi:10.1029/JB076i002p00570.

Davis, E. E., Lister, C. R. B., 1974. Fundamentals of ridge crest topography. Earth Planet. Sci. Let. 21, 405-413.

Davies, G. F., 1980. Review of oceanic and global heat flow estimates. Rev. Geophys. Space Phys. 18, 718-722.

Ernst, R. E., Buchan, K. L., 2003. Recognizing mantle plumes in the geological record. Annu. Rev. Earth Planet. Sci. 31, 469-523.

Faccenda, M., Burlini, L., Gerya, T. V., Mainprice, D., 2008. Fault-induced seismic anisotropy by hydration in subducting oceanic plates. Nature 455, 1097-1100, doi:10.1038/nature07376.

Hirano, N., Kawamura, K., Hattori, M., Saito, K., Ogawa, Y., 2001. A new type of intra-plate volcanism; young alkali-basalts discovered from the subducting Pacific Plate, northern Japan Trench. Geophys. Res. Lett. 28, 2719-2722.

Hirano, N., Yamamoto, J., Kagi, H., Ishii, T., 2004. Young, olivine xenocryst-bearing alkali basalt from the oceanward slope of the Japan Trench. Contrib. Minaral. Petrol. 148, 47-54.

Hirano, N., Takahashi, E., Yamamoto, J., Abe, N., Ingle, S.P., Kaneoka, K., Kimura, J., Hirata, T., Ishii, T., Ogawa, Y., Machida, S., Suyehiro, K., 2006. Volcanism in response to plate flexure. Science 313, 1426-1428.

Hirano, N., Koppers, A.A.P., Takahashi, A., Fujiwara, T., Nakanishi, M., 2008. Seamounts, knolls and petit-spot monogenetic volcanoes on the subducting Pacific Plate. Basin Res. 20, 543–553.

Holtzman, B. K., Kohlstedt, D. L., Zimmerman, M. E., Heidelbach, F., Hiraga, T., Hustoft, J., 2003. Melt segregation and strain partitioning: implications for seismic anisotropy and mantle flow. Science 301, 1227-1230.

Jung, H., Katayama, I., Jiang, Z., Hiraga, T., Karato, S., 2006. Effect of water and stress on the lattice-preferred orientation of olivine. Tectonophysics 421, 1–22.

Jung, H., Mo, W. Green, H. W., 2008. Upper mantle seismic anisotropy resulting from pressure-induced slip transition in olivine. Nature Geoscience 2, 74-77.

Kawakatsu, H., Kumar, P., Takei, Y., Shinohara, M., Kanazawa, T., Araki, E., Suyehiro, K., 2009. Seismic evidence for sharp lithosphere–asthenosphere boundaries of oceanic plates. Science 324, 499–502.

Le Roux, V., Bodinier, J.L., Tommasi, A., Alard, O., Dautria, J.M., Vauchez, A., Riches, A., 2007. The Lherz spinel–lherzolite: refertilized rather than pristine mantle. Earth Planet. Sci. Lett. 259, 599–612, doi:10.1016/j.epsl.2007.05.026.

Le Roux, V., Tommasi, A., Vauchez, A., 2008. Feedback between melt percolation and deformation in an exhumed lithosphere–asthenosphere boundary. Earth Planet. Sci. Lett. 274, 401–413.

Long, M. D., Silver, P. G., 2009. Shear Wave Splitting and Mantle Anisotropy: Measurements, Interpretations, and New Directions. Surv. Geophys. 30, 407–461, DOI:10.1007/s10712-009-9075-1.

Mainprice, D., 1990. A FORTRAN program to calculate seismic anisotropy from the lattice preferred orientation of minerals, Comput. Geosci. 16, 385–393, doi:10.1016/0098-3004 (90)90072-2.

Mainprice, D., Barruol, G., Ben Ismaíl, W., 2000. The anisotropy of the Earth's mantle: From single crystal to polycrystal, in: Karato, S. –I., Forte, A. M., Liebermann, R. C., Masters, G., Stixrude, L. (Eds.), Earth's Deep Interior: Mineral Physics and Tomography From the Atomic Scale to the Global Scale, Geophysical Monograph Series vol. 117. American Geophysical Union, Washington, D. C., pp. 237–264.

Mainprice, D., Tommasi, A., Couvy, H., Cordier, P., Frost, D. J., 2005. Pressure sensitivity of olivine slip systems and seismic anisotropy of the Earth's upper mantle. Nature 233, 731–733, doi:10.1038/nature03266.

Mainprice, D., 2007. Seismic anisotropy of the deep Earth from a mineral and rock physics perspective. In: Schubert, G. (Eds.), Treatise in Geophysics, Volume 2. Oxford, UK: Elsevier, pp. 437–492.

McKenzie, D. P., 1967. Some remarks on heat flow and gravity anomalies. J. Geophys. Res. 72, 6262-6271.

Mehl, L., Hacker, B. R., Hirth, G., Kelemen, P. B., 2003. Arc-parallel flow within the mantle wedge: evidence from the accreted Talkeena arc, south central Alaska. J. Geophys. Res. 108, doi:10.1029/2002JB002233.

Michibayashi, K., Mainprice, D., 2004. The role of preexisting mechanical anisotropy on shear zone development within oceanic mantle lithosphere: An example from the Oman ophiolite. J. Petrol. 45, 405–414, doi:10.1093/ petrology/egg099.

Molnar, P., Stock, J., 1987. Relative motionsof hotspots in Pacific, Atlantic and Indian Oceans since late Cretaceous time. Nature 327(6123), 587-591.

Nagumo, S., Kubo, A., Ouchi, T., Katao, H., Koresawa, S., 1990. Report on DELP 1986 cruise in the northwestern Pacific 3: seismic structure revealed by explosion experiments. Bull. Earthq. Res. Inst., Univ. Tokyo 65, 89-104.

Nicolas, A., 1986. Structure and petrology of peridotites: Clues to their geodynamic environment. Rev. Geophys. 24, 875-895.

Nicolas, A., Christensen, N. I., 1987. Formation of anisotropy in upper mantle peridotite: a review. In: Fuchs, K., Froidevaux, C. (Eds.), Composition Structure and Dynamics of the Lithosphere-Asthenosphere System, Geodynamics Monograph Series vol. 16, American Geophysical Union, Washington, D. C., pp. 111-123.

Nicolas, A., Poirier, J. P., 1976. Crystalline Plasticity and Solid State Flow in Metamorphic Rocks. John Wiley, London.

Nicolas, A., Boudier, F., Boullier, A. M., 1973. Mechanism of flow in naturally and experimentally deformed peridotites. Am. J. Sci. 273, 853-876.

Nicolas, A., 1989. Structures of Ophiolites and Dynamics of Oceanic Lithosphere. Kluwer Academic Publishers, Dordrecht.

O'Neill, H., 1981. The transition between spinel lherzolite and garnet lherzolite, and its use as a geobarometer. Contrib. Mineral. Petrol. 77, 185–194.

Ouchi, T., Nagumo, S., 1990. Explosion for crustal and mantle structure at the Pacific Ocean. Chikyu 12(5), 262-266 (in Japanese).

Park, J., Levin, V., 2002. Seismic anisotropy: Tracing plate dynamics in the mantle. Science 296, 485-489.

Parsons, B., Sclater, J. G., 1977. An analysis of the variation of ocean floor bathymetry and heat flow with age. J. Geophys. Res. 82(5), 803-827.

Pera, E., Mainprice, D., Burlini, L., 2003. Anisotropic seismic properties of the upper mantle beneath the Torre Alfina area (North Apennines, Central Italy). Tectonophysics 370, 11-30.

Satsukawa, T., Michibayashi, K., 2009. Determination of slip system in olivine based on crystrallographic preferred orientation and subgrain rotation axis: examples from Ichinomegata peridotite xenoliths, Oga peninsula, Akita prefecture (in Japanese with the English abstract). Jour. Geol. Soc. Japan. 115(6), 288-291.

Savage, M. K., 1999. Seimic anisotropy and mantle deformation: What have we learned from shear wave splitting? Rev. Geophys. 37, 65-106.

Sen, G., Keshav, S., Bizimis, M., 2005. Hawaiian mantle xenoliths and magmas: Composition and thermal character of the lithosphere. Am. Mineral. 90, 871-887.

Sharp, W. D., Clague, D. A., 2006. 50-Ma Initiation of Hawaiian-Emperor Bend Records Major Change in Pacific Plate Motion. Science 313, 1281-1284, DOI: 10.1126/science.1128489.

Shimamura, H., Asada, T., Suehiro, K., Yamada, T., Inatani, H., 1983. Longshot experiments to study velocity anisotropy in the oceanic lithosphere of the northwestern Pacific. Phys. Earth Planet. Int. 31, 348-362.

Shimamura, H., Asada, T., 1984. Velocity anisotropy extending over the entire depth of the oceanic lithosphere. In: Hilde, T. W. C., Uyeda, S. (Eds.), Geodynamics Monograph Series vol. 11. American Geophysical Union, Washington, D. C., pp. 121–125.

Shinohara, M., Fukano, T., Kanazawa, T., Araki, E., Suyehiro, K., Mochizuki, M., Nakahigashi, K., Yamada, T., Mochizuki, K., 2008. Upper mantle and crustal seismic structure beneath the Northwestern Pacific Basin using a seafloor borehole broadband seismometer and ocean bottom seismometers. Phys. Earth Planet. Int. 170, 95–106

Stein, C. A., Stein, S., 1992. A model for the global variation in oceanic depth and heat flow with lithospheric age. Nature 359, 123-129.

Suhr, G., 1993. Evaluation of upper mantle microstructures in the Table Mountain massif (Bay of Islands ophiolites). J. Struct. Geol. 15, 1273-1292.

Takahashi, E., 1986. Origin of basaltic magmas - implications from peridotite melting experiments and an olivine fractionation model. Bull. Volcanol. Soc. Japan 30, 17–40.

Tasaka, M., Michibayashi, K., Mainprice, D., 2008. B-type olivine fabrics developed in the fore-arc side of the mantle wedge along a subducting slab. Earth. Planet. Sci. Lett. 272, 747-757.

Tommasi, A., Tikoff, B., Vauchez, A., 1999. Upper mantle tectonics: three-dimensional deformation, olivine crystallographic fabrics and seismic properties. Earth Planet. Sci. Lett. 168, 173-186.

Tommasi, A., Mainprice, D., Canova, G., Chastel, Y., 2000. Viscoplastic self-consistent and equilibrium-based modeling of olivine lattice preferred orientations. Implications for upper mantle seismic anisotropy. J. Geophys. Res. 105, 7893-7908.

Tommasi, A., Godard, M., Coromina, G., Dautria, J. -M., Barsczus, H., 2004. Seismic anisotropy and compositionally induced velocity anomalies in the lithosphere above mantle plumes: a petrological and microstructural study of mantle xenoliths from French Polynesia. Earth Planet. Sci. Lett. 227(3–4), 539–556.

Tommasi, A., Vauchez, A., Godard, M., Belley, F., 2006. Deformation and melt transport in a highly depleted peridotite massif from the Canadian Cordillera: Implications to seismic anisotropy above subduction zones. Earth Planet. Sci. Lett. 252, 245–259. doi:10.1016/j.epsl.2006.09.042.

Tommasi, A., Vauchez, A., Ionov, D. A., 2008. Deformation, static recrystallization, and reactive melt transport in shallow subcontinental mantle xenoliths (Tok Cenozoic volcanic field, SE Siberia). Earth Planet. Sci. Lett. 272, 65-77, doi:10.1016/j.epsl.2008.04.020.

Turcotte, D. L., Schubert, G., 1982. Geodynamics, first ed. John Wiley & Sons, Inc., New York.

Vauchez, A., Garrido, C., 2001. Seismic properties of an asthenospherized lithospheric mantle: constraints from lattice preferred orientations in peridotite from the Ronda massif. Earth Planet. Sci. Lett. 192, 235–249.

Vauchez, A., Dineur, F., Rudnick, R., 2005. Microstructure, texture and seismic anisotropy of the lithospheric mantle above a mantle plume: Insights from the Labait volcano xenoliths (Tanzania). Earth Planet. Sci. Lett. 232(3–4), 295–314.

Vonlanthen, P., Kunze, K., Burlini, L., Grobéty, B., 2006. Seismic properties of the upper mantle beneath Lanzarote (Canary Islands): model predictions based on texture measurements by EBSD. Tectonophysics 428, 65–86.

Wells, P. R. A., 1977. Pyroxene thermometry in simple and complex systems. Contrib. Mineral. Petrol. 62, 129–139.

Yamamoto, J., Kagi, H., 2006. Extended Micro-Raman Densimeter for CO_2 Applicable to Mantle-originated Fluid Inclusions. Chem. Lett. 35 (6), 610-611.

Yamamoto, J., Hirano, N., Abe, N., Hanyu, T., 2009. Noble gas isotopic compositions of mantle xenoliths from northwestern Pacific lithosphere. Chem. Geol. 268, 313–323.

Zhang, S., Karato, S. -I., 1995. Lattice preferred orientation of olivine aggregates in simple shear. Nature 375, 774-777.

Zhang, S., Karato, S. –I., FitzGerald, F., Faul, U. H., Zhou, Y., 2000. Simple shear deformation of olivine aggregates. Tectonophysics 316, 133-152.

Zimmerman, M. E., Zhang, S., Kohlstedt, D. L., Karato, S. -I., 1999. Melt distribution in mantle rocks deformed in shear. Geophys. Res. Lett. 26, 1505-1508.

Figure captions

Fig. 1. (a) Bathymetric map of the NW Pacific Ocean, showing the surveyed area (white rectangle; Site A of Hirano et al., 2006) and the sampling point at dive site 6K#880 (star). The sample was dredged from the eastern fault escarpment of petit-spot volcanoes in the Japan Trench. (b) Enlargement of Site A. The red star indicates the site where sample 6K#880R2O was obtained during a dive as part of cruise YK05-06 (R/V *Yokosuka* and the submersible *Shinkai 6500*; dive site 6K#880). Topographic data are from Amante and Eakins (2008).

Fig. 2. Schematic image and sample photos of the analyzed peridotite xenolith in this study. Black ellipses show mineral SPO such as olivine and pyroxene in schematic image. Elongated pyroxene and olivine grains in hand spaceman oriented parallel to foliation.

Fig. 3. (a) Microphotograph of microstructure within the petit-spot peridotite xenolith (6K880R02) collected from Site A of Hirano et al. (2006). Cross polarized light. (b) Line diagram of the microstructures seen in (a); white is olivine, light grey is orthopyroxene, dark grey is clinopyroxene, black is the reaction zone between host rock and peridotite, and the hatched area is a fine-grained spinel–orthopyroxene aggregate. (c) Crystallographic preferred orientation map (data collected by EBSD) of olivine in (a), showing an Inverse Pole Figure (IPF) in color, as compiled using Channel+5 software (HKL Technology). White areas represent other phases (e.g., orthopyroxene and clinopyroxene) that could not be indexed (i.e., a zero solution). Ol = olivine, Opx = orthopyroxene, Cpx = clinopyroxene.

Fig. 4. (a) Microphotograph of olivine microstructure. Olivine grains show features of for intra-crystalline deformation, such as subgrain boundaries. Cross polarized

light. (b) Back-scatted electron image (BEI) of the fine-grained spinel–orthopyroxene aggregate, outlined by the white broken line, in the petit-spot peridotite xenolith. The aggregate has a roundish equidimensional shape. (c) Enlargement of the area outlined by the yellow rectangle in (b). The outer parts are coarse-grained and granular with many cracks, whereas the inner parts are very fine-grained with fine cracks. Ol = olivine, Opx = orthopyroxene, Cpx = clinopyroxene, Sp = spinel.

Fig. 5. (a) Crystallographic preferred orientation (CPO) data for olivine, orthopyroxene, and clinopyroxene are plotted at equal-area, lower-hemisphere projections. Contours are multiples of uniform density. PfJ is the fabric intensities in each pole figure calculated after Mainprice et al. (2000) and Michibayashi and Mainprice (2004). (b) Seismic properties calculated from single crystal elastic constants, crystal density, and the CPOs of olivine, orthopyroxene, and clinopyroxene at 20 kbar and 1100ºC. Vp is the 3D distribution of P-wave velocity. Contours are multiples of uniform density. AVs is the 3D distribution of the polarization anisotropy of S-waves due to S-wave splitting. The Vs1 plane is the polarization plane of the fast split S-wave (S1). Color shading for AVs is also shown. Contours for Vp are in km/s, while those for AVs are in % anisotropy, as is the trace of the Vs1 polarization plane.

Figure

Click here to download Figure: Petit-figure.doc

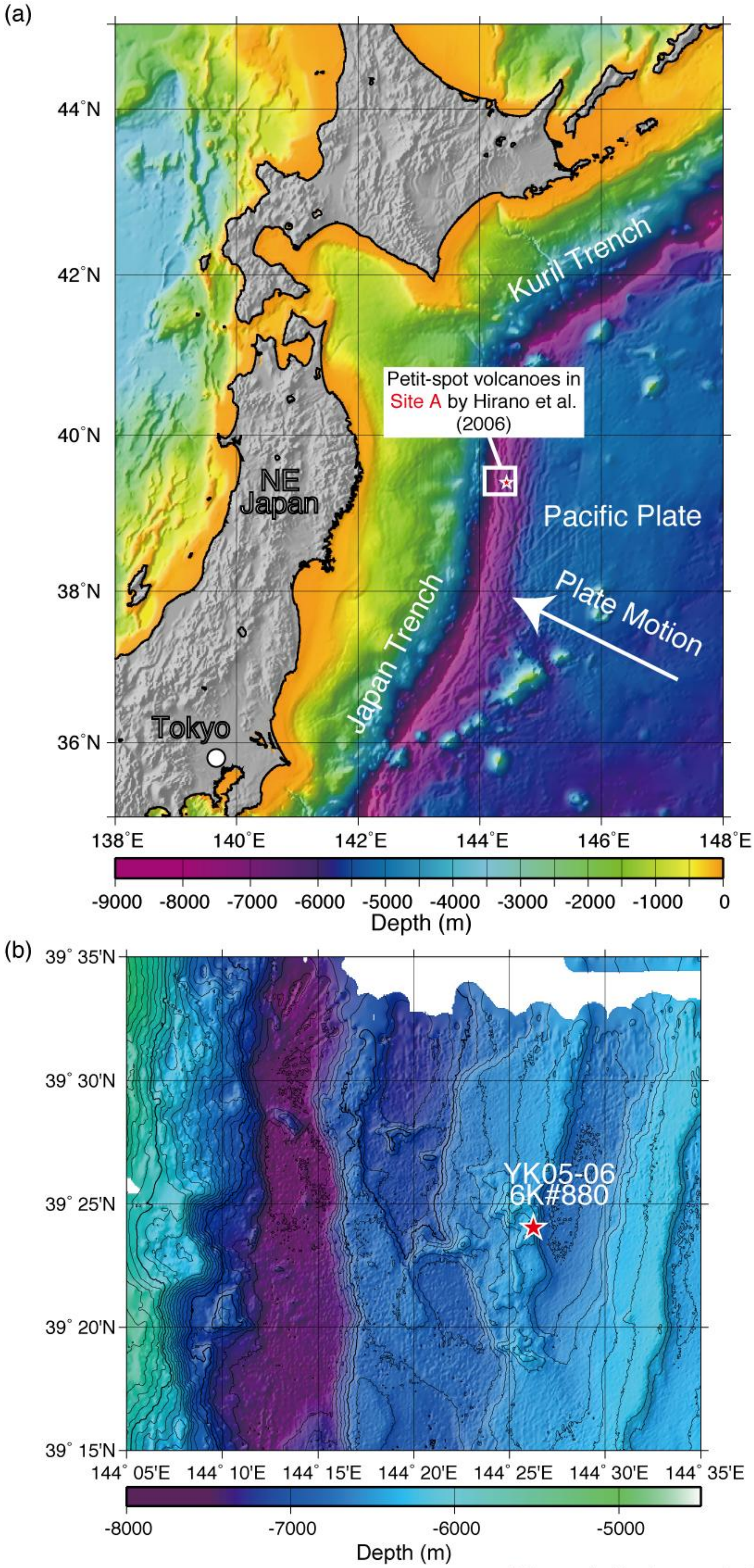

Figure 1. Harigane et al.

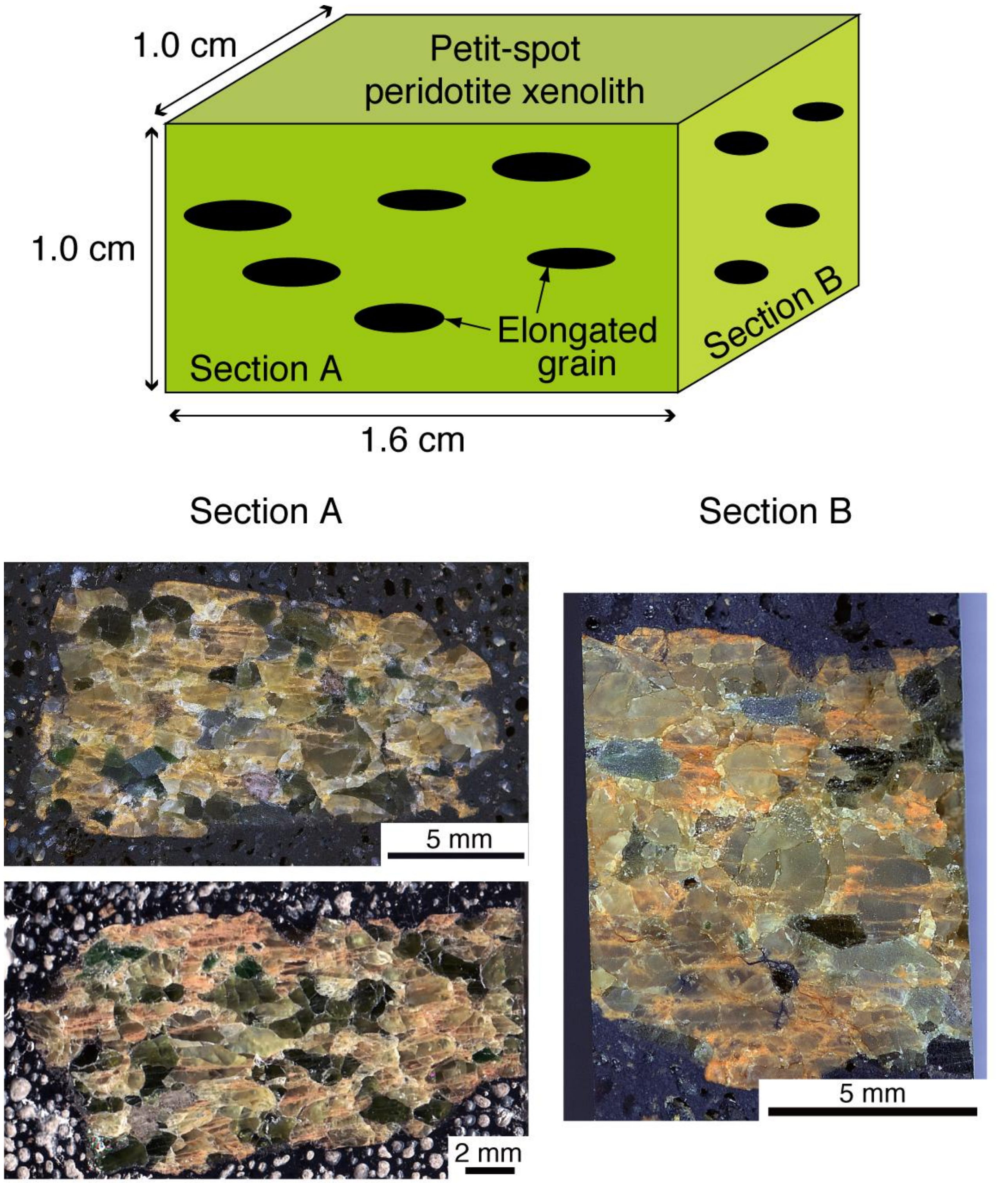

Figure 2. Harigane et al.

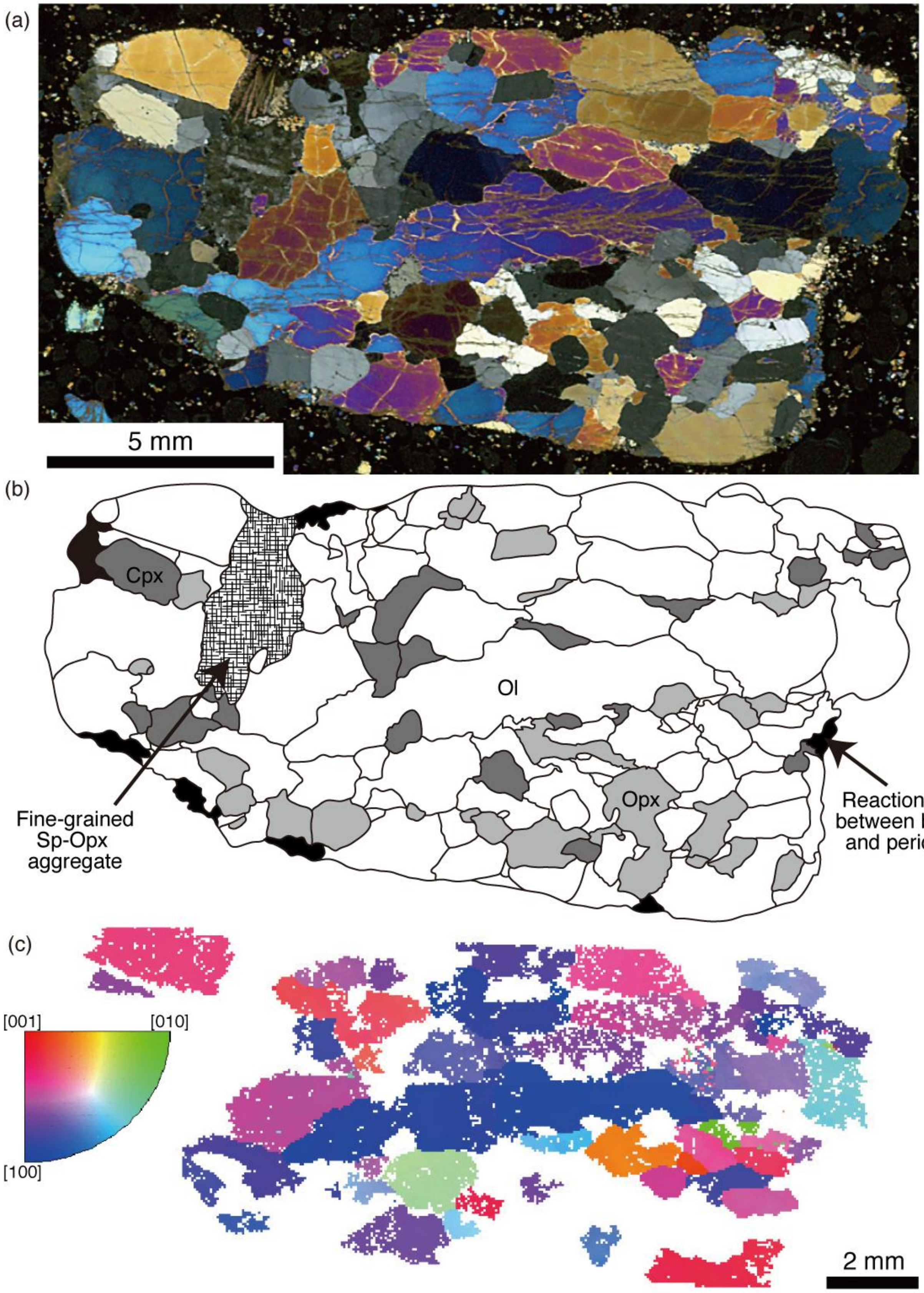

Figure 3. Harigane et al.

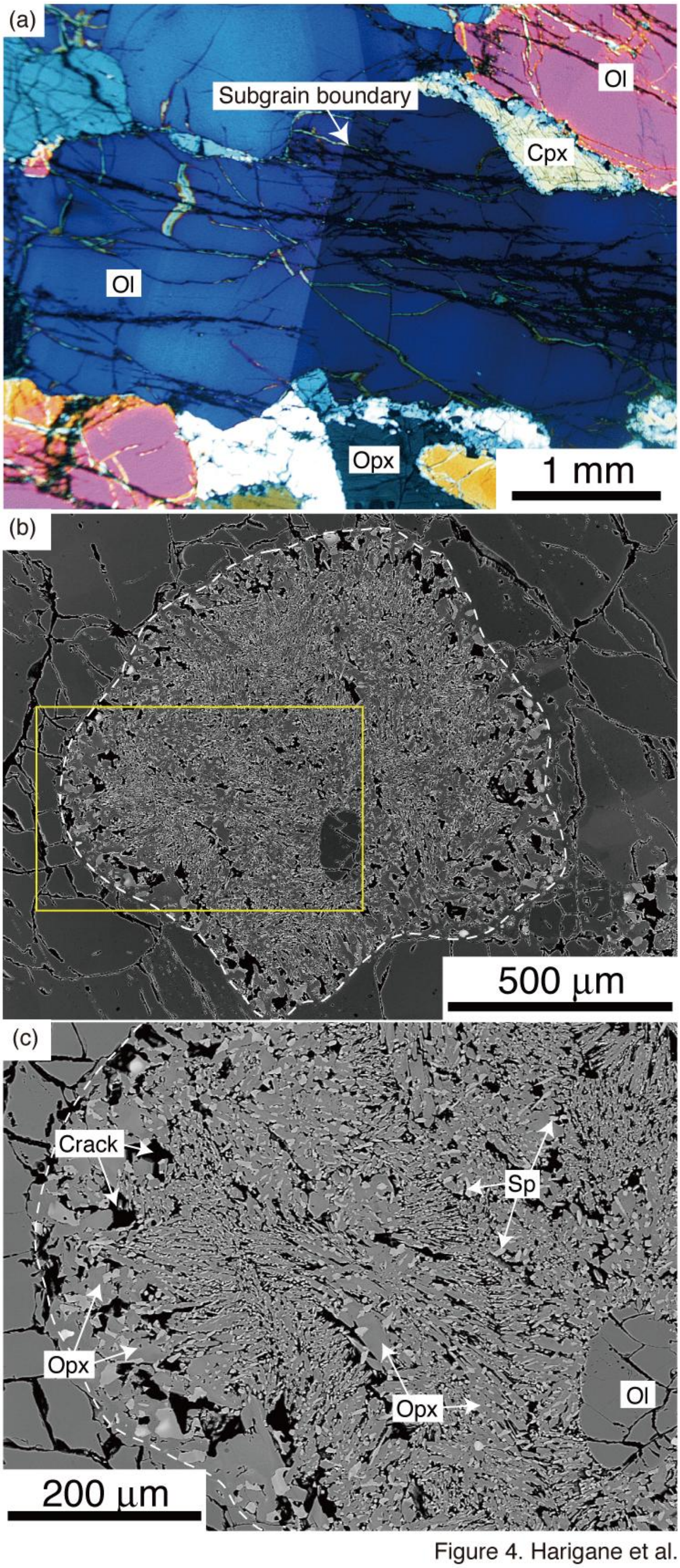

Figure 4. Harigane et al.

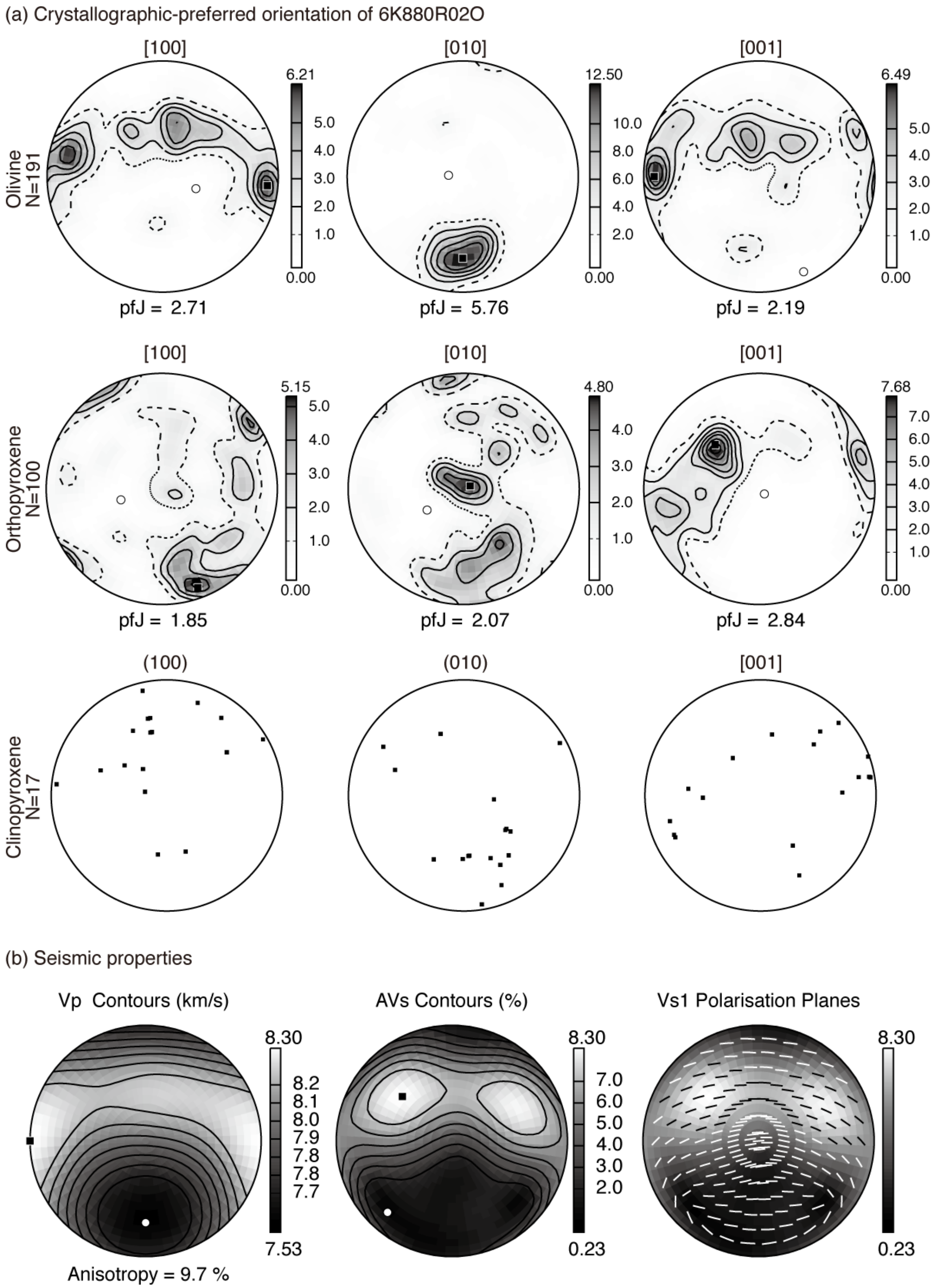

Figure 5. Harigane et al.